
A MODEL FOR POSITRON ANNIHILATION IN MULTI-LAYER SYSTEMS BY SOLVING THE DIFFUSION EQUATION USING DIFFERENT POSITRON AFFINITIES

A PREPRINT

Lucian Mathes^{*1,2}, Michael Gödl^{1,2}, Michael Leitner¹, Bettina Kohlhaas¹, Maximilian Suhr^{1,2}, Vassily Vadimovitch Burwitz^{1,2,3}, Armin Manhard³, and Christoph Hugenschmidt¹

¹Heinz Maier-Leibnitz Zentrum (MLZ), Technical University of Munich, Lichtenbergstr. 1, 85748 Garching, Germany

²School of Natural Sciences, Physics Department, Technical University of Munich, James-Franck-Str. 1, 85748 Garching, Germany

³Max Planck Institute for Plasma Physics, Boltzmannstr. 2, 85748 Garching, Germany

November 6, 2025

ABSTRACT

We present a method for solving the positron diffusion equation in multi-layer systems. Our approach incorporates material-specific implantation profiles, diffusion parameters, and positron affinities. It utilizes a Markov chain approach to model annihilation probabilities and provides fitting capabilities for experimental S (lineshape) parameter data. We have implemented this algorithm in Python and made it available for free under the name LIMPID. To demonstrate its performance, we analyze depth-resolved Doppler-Broadening Spectroscopy measurements of a Cu layer on a Si substrate, achieving excellent agreement with the experimental profiles. The LIMPID tool enhances the reproducibility and comparability of positron defect characterization measurements across different research groups.

Keywords Positron annihilation · Positron diffusion · Doppler-broadening spectroscopy

1 Introduction

Positron Annihilation Spectroscopy (PAS) is a well-established and highly sensitive technique used to study atomic-level defects in solid materials. After implantation, positrons rapidly thermalize in the crystal lattice [SL88]. Once thermalized, they diffuse through the lattice with a diffusion length that strongly depends on the defect concentration [PN94]. Finally, the positron annihilates with an electron by the emission of gamma radiation, in most cases consisting of two 511 keV photons. The lifetime of positrons depends on the local electron density, while the energy of the annihilation radiation provides insights into the electron momentum distribution. This information, in turn, reveals the nature of defects present in the material. PAS is particularly sensitive to distinguishing between delocalized positrons annihilating in a defect-free lattice and positrons that are trapped in lattice imperfections such as vacancies, dislocations, and voids [Číž18].

A widely used method within PAS is Doppler-Broadening Spectroscopy (DBS) of the positron-electron annihilation line. The annihilating electrons transfer their momentum to the annihilation photons (the momentum of the thermalized positrons is negligible). The electron momentum distribution, hence, leads to Doppler-shifted annihilation photons, which produce a Doppler-broadened annihilation photo peak in the recorded gamma spectrum. The broadening of the annihilation peak, which differs between defect-free bulk and defects, is commonly quantified by the lineshape parameter, S , which represents the fraction of events within a defined low-momentum region around the center of

^{*}lucian.mathes@tum.de

the Doppler-broadened annihilation peak. By employing monoenergetic positron beams, depth-resolved DBS measurements can be performed. These allow the measurement of the S parameter as a function of positron implantation energy, $S(E)$, and hence the investigation of, e.g., near-surface region defects, layered structures, and defect profiles. The $S(E)$ profile contains information about the thickness of layers as well as the positron diffusion length in each layer and thus the defect concentration.

Due to the diffusion of thermalized positrons before annihilation, the annihilation profile, i.e., the number of positrons that annihilate in each layer and at the surface, differs from the implantation profile. The diffusion behavior of positrons is influenced by various material properties, including defect concentration, layer structures, and positron affinity. To accurately extract defect-related parameters from depth-resolved DBS experiments, it is necessary to solve the positron diffusion equation, which describes how positrons migrate through the material before annihilation. Since complex boundary conditions and material-specific properties can influence diffusion, numerical modeling is often required to interpret experimental data effectively. Layer-wise Investigation of Measurements on Positron Implantation and Diffusion (LIMPID) is a computational tool specifically developed to solve this diffusion problem efficiently across a wide range of systems and boundary conditions. While the diffusion length, from which the vacancy concentration can be determined, is typically the primary output of LIMPID, other material parameters – such as layer thicknesses or positron affinities – can also be fitted, provided that a sufficient number of known/fixed parameters is available.

Depth-resolved DBS relies on the implantation of monoenergetic positrons into a sample, resulting in a broad, peak-shaped implantation profile. Since positrons diffuse within the material before annihilation, accurately modeling their diffusion behavior is crucial for interpreting data from depth-resolved DBS experiments. The LIMPID algorithm is specifically designed to solve the diffusion problem for thermalized positrons in solid materials.

Starting from a given positron implantation profile as described by, e.g., Makhov [AL90; Mak60], LIMPID models the positron diffusion and returns an S parameter value for each individual positron implantation energy. We have implemented an optional correction for epithermal positrons at low positron implantation energies. In the case of layered structures, LIMPID accounts for multiple layers of varying thicknesses, as well as material-dependent diffusivities, lifetimes, S parameter, and positron affinities.

To ensure accessibility and auditability of use for researchers across different scientific disciplines, LIMPID was implemented in Python and published as open-source². Python was chosen due to its widespread adoption in the scientific community, the extensive ecosystem of numerical and data analysis libraries, and its user-friendly syntax. The algorithm represents samples in a class-based digital structure, allowing users to input and access experimental parameters and sample properties as class attributes. For parameter estimation and curve fitting, LIMPID leverages the lmfit library [New+24], which provides a framework for non-linear least-squares fitting. The core numerical computations rely on NumPy [Har+20] and SciPy [Vir+20]. Matplotlib [Hun07] handles the visualization of results.

LIMPID was developed to support positron research groups in data analysis, aiming to replace both an earlier tool introduced by van Veen [Vee+91] and the many custom-built and unpublished scripts tailored to specific experimental setups and sample structures. By providing a unified, improved, expandable, and open-source solution, LIMPID enhances the transparency, reproducibility, and comparability of depth-resolved DBS analyses across research groups. The algorithm has already been successfully applied, as demonstrated in recent publications [Sch+24; Bur+25].

2 Method / Algorithm

Positrons with a given kinetic energy interact with the sample material, losing energy through inelastic collisions. This process, known as thermalization, continues until the positrons reach thermal equilibrium with their surroundings, at an energy of approximately 40 meV at room temperature.

- 1. Positron implantation:** Initially, positrons are implanted into the material. The depth distribution is calculated using an implantation model (here: Makhov) and a set of material-dependent parameters.

The transport of thermalized positrons in a solid is modeled using diffusion theory. In LIMPID, the sample is modelled via a number of homogeneous layers of arbitrary thickness and positron-relevant properties. The trajectory of a given positron is conceptually divided into segments corresponding to its residing in the individual sample layers. The resulting mathematical problem is thus solved in two stages:

²LIMPID is licensed under the GNU General Public License v3.0. Source code available at <https://github.com/lucianmathes/limpid>.

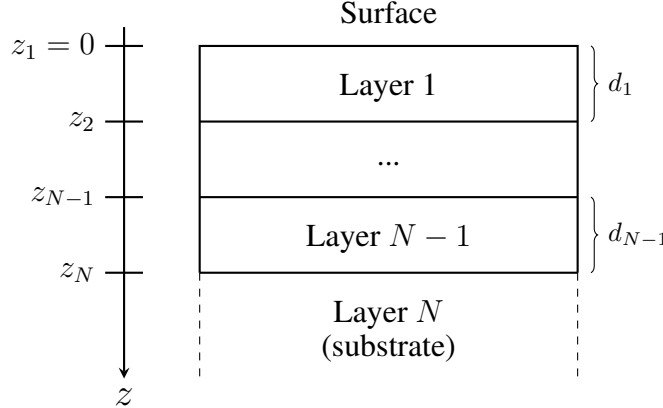


Figure 1: Schematic drawing of a generic sample explaining the nomenclature used by LIMPID. The sample consists of N layers, whereby the N^{th} layer has an infinite thickness.

2. **Diffusion to the layer boundaries:** After thermalization, positrons diffuse through the material via random thermal motion, eventually either annihilating within a layer or reaching an interface between layers. In a homogeneous sample, this process simplifies to positron diffusion to the surface or annihilation in the bulk.
3. **Jumping between layer boundaries:** For those positrons that reach a boundary before annihilating, the subsequent trajectory is modeled as a Markov process. It is defined by the probabilities of annihilating within one of the two adjacent layers or reaching one of the two neighbouring boundaries, tracking how positrons move through the material until they eventually disappear.

Both steps include positron annihilation at various depths within the material, resulting in an annihilation profile that reflects the contribution of positrons from each layer or the surface to the measured signal. From this profile, LIMPID calculates a weighted S parameter from the layer- and surface-specific S parameters. Figure 1 shows a schematic drawing of a generic sample clarifying the nomenclature and indexing used in the following.

2.1 Positron Implantation

Positron implantation and thermalization are complex and consist of many particle-particle interactions. The distribution of thermalized positrons, i.e., the implantation profile, at a given energy E is already broad and can be approximated by its width $\propto E^{1.62}$ [Veh+87]. Typically, the Makhov distribution is employed to model the implantation profile [AL90; Mak60], although more sophisticated models also exist [Gho95]. Parameters for a variety of materials have been determined through Monte Carlo simulations and are publicly available [DH08; PN94]. Multi-layer implantation profiles are combined from the individual material-specific implantation profiles scaled with the correct fractions [Aer94]. LIMPID currently includes the Makhov implantation profile described by:

$$P(z) = \frac{mz^{m-1}}{z_0^m} \exp \left[-\left(\frac{z}{z_0} \right)^m \right], \quad (1)$$

with

$$z_0 = \frac{A}{\rho \Gamma(1 + \frac{1}{m})} E^n, \quad (2)$$

where m , n and A are material-specific parameters, ρ is the material density and E is the positron implantation energy. Two example profiles for a layered system are shown in Figure 5.

2.2 Diffusion to the Layer Boundaries

The one-dimensional diffusion equation inside layer i is given by

$$\frac{\partial n(z, t)}{\partial t} = D_i \frac{\partial^2 n(z, t)}{\partial z^2} - \lambda_{\text{eff},i} n(z, t), \quad (3)$$

where $n(z, t)$ is the positron density as a function of time t and depth z , D_i is the diffusion coefficient, and $\lambda_{\text{eff},i}$ is the effective annihilation rate,

$$\lambda_{\text{eff},i} = \frac{1}{\tau_{\text{eff},i}} = \lambda_{\text{bulk},i} + \kappa c_i, \quad (4)$$

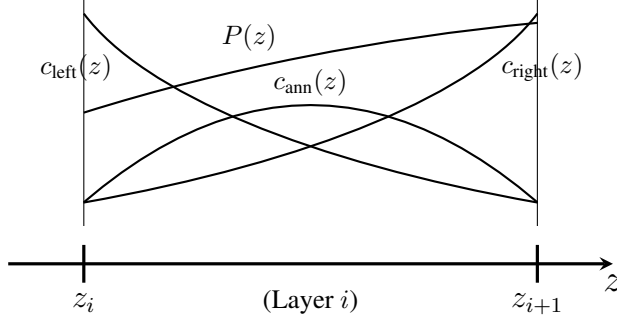


Figure 2: Schematic drawing of the first diffusion step inside the i^{th} layer. $P(z)$ represents the positron implantation profile within a material layer of thickness d . After diffusion, the positron distribution at the layer boundaries is determined by integrating the product of $P(z)$ and the probability of a positron reaching the left [right] boundary $c_{\text{left}}(z)$ [$c_{\text{right}}(z)$]. The corresponding mathematical formulation is provided in Equation 6. c_{ann} is the probability of a positron to annihilate before reaching a boundary. All three probabilities sum to 1.

where $\lambda_{\text{bulk},i}$ is the annihilation rate of positrons in the defect-free bulk, κ is the specific trapping rate of a defect, and c_i is the defect concentration inside layer i . In the case of multiple types of defects, j , present in the layer, κc_i becomes $\sum_j \kappa_j c_{j,i}$ representing an “effective” defect with “effective” S parameter.

Under steady-state conditions, we get

$$0 = D_i \frac{d^2 n(z)}{dz^2} - \lambda_{\text{eff},i} n(z) + \mu P(z, E), \quad (5)$$

where $P(z, E)$ is the implantation profile for energy E and $\mu = 1 \text{ s}^{-1}$ is the positron flux. Note that all positron fractions calculated in the following are independent of the value for μ . Solving Equation 5 gives the fraction of positrons diffusing to the left (low z) layer boundary instead of directly annihilating or reaching first the right boundary:

$$f_{\text{left},i} = \int_{z_i}^{z_{i+1}} P(z, E) c_{\text{left},i}(z) dz = \int_{z_i}^{z_{i+1}} P(z, E) \frac{\sinh[u_i(z_{i+1} - z)]}{\sinh[u_i(z_{i+1} - z_i)]} dz, \quad (6)$$

where $c_{\text{left},i}(z)$ is the probability of a positron at position z diffusing to the left boundary (as plotted in the explanatory graphic in Figure 2) and $z_{i+1} - z_i$ is equal to the layer thickness; u_i is the inverse positron diffusion length inside layer i :

$$u_i = \sqrt{\frac{\lambda_{\text{eff},i}}{D_i}} = \frac{1}{L_i}. \quad (7)$$

We get the fraction of positrons diffusing to the right (high z) layer boundary, $f_{\text{right},i}$, by replacing $c_{\text{left},i}(z)$ with

$$c_{\text{right},i}(z) = \frac{\sinh[u_i(z - z_i)]}{\sinh[u_i(z_{i+1} - z_i)]}. \quad (8)$$

The fraction of positrons annihilating inside the i^{th} layer is then

$$f_{\text{ann},i} = 1 - f_{\text{left},i} - f_{\text{right},i}. \quad (9)$$

2.3 Diffusion Between Layer Boundaries

After the initial diffusion step, which is essentially the set-up for the second/main diffusion step, the diffusion equation simplifies. Now, positrons that reach a boundary can either transition to an adjacent boundary or annihilate. Note that positrons can only annihilate inside layers or at the surface, but not at the infinitesimally thin layer boundaries, which are assumed not to trap positrons. (Interfaces with high positron affinity/attractiveness trapping positrons – e.g., due to lattice mismatch – can be modelled as additional thin layers.) This process follows

$$0 = D_i \frac{d^2 n(z)}{dz^2} - \lambda_{\text{eff},i} n(z), \quad (10)$$

where D_i is the diffusion coefficient and $\lambda_{\text{eff},i}$ is the effective annihilation rate for the material of layer i . We define the positron density at the layer boundary z_i as

$$n(z_i) = n_0 \quad (11)$$

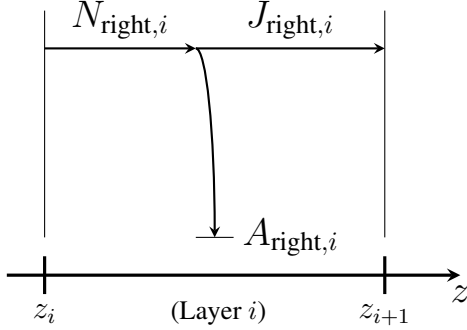


Figure 3: Schematic drawing of the fluxes in the second diffusion step. After reaching a layer boundary, positrons either jump between boundaries or annihilate within the layer. The transition probabilities calculated from the fluxes form a Markov chain, which describes how positrons move through the system until they are annihilated.

with units positrons/m. The solution of the diffusion equation is then

$$n(z) = n_0 \frac{\sinh[u_i(z - z_{i+1})]}{\sinh[u_i(z_i - z_{i+1})]}. \quad (12)$$

We get the flux of positrons leaving the boundary towards the right (with units positrons/s) using Fick's first law of diffusion and the right-sided derivative:

$$N_{\text{right},i} = -D_i \left. \frac{dn(z)}{dz} \right|_{z=z_i^+} = n_0 u_i D_i \frac{\cosh[u_i(z_{i+1} - z_i)]}{\sinh[u_i(z_{i+1} - z_i)]}. \quad (13)$$

The flux of positrons that reach the next (right-sided) layer boundary is given by the left-sided derivative at z_{i+1} :

$$J_{\text{right},i} = -D_i \left. \frac{dn(z)}{dz} \right|_{z=z_{i+1}^-} = \frac{n_0 u_i D_i}{\sinh[u_i(z_{i+1} - z_i)]}. \quad (14)$$

The amount of positrons annihilating on the way results from the difference between the two fluxes:

$$A_{\text{right},i} = N_{\text{right},i} - J_{\text{right},i}. \quad (15)$$

Same applies to the left-sided diffusion and annihilation, where we obtain the fluxes $N_{\text{left},i}$, $J_{\text{left},i}$, and $A_{\text{left},i}$ by exploiting the symmetry of the diffusion process:

$$A_{\text{left},i} = A_{\text{right},i-1}, \quad (16)$$

where i is the layer boundary index. Same applies to $J_{\text{right/left}}$ and $N_{\text{right/left}}$. We normalize those fluxes ($n_0 = 1$) to get the probabilities of a positron diffusing to the next boundary and a positron annihilating on the way:

$$j_{\text{right},i} = \frac{J_{\text{right},i}}{N_{\text{right},i} + N_{\text{left},i}}, \quad (17)$$

(equivalently for j_{left} , a_{right} , and a_{left}). Note that the resulting probabilities depend on the diffusion and annihilation characteristics of both adjacent layers ($u_{i-1} D_{i-1}$ and $u_i D_i$).

We use a time-homogeneous Markov chain with a finite state space to describe the diffusion between layer boundaries. The layer boundaries (plus the surface) are transient states, while the layers themselves (plus the surface) are absorbing states. We implement this Markov process using matrices. The matrix, \mathbf{Q} , is filled with the probabilities of transitions between transient states, i.e., positrons jumping from one layer boundary to another (including the surface). For example, with 4 layers and therefore 3 layer boundaries (plus the surface), we get

$$\mathbf{Q} = \begin{pmatrix} 0 & j_{\text{left},1} & 0 & 0 \\ j_{\text{right},0} & 0 & j_{\text{left},2} & 0 \\ 0 & j_{\text{right},1} & 0 & j_{\text{left},3} \\ 0 & 0 & j_{\text{right},2} & 0 \end{pmatrix}, \quad (18)$$

where the $j_{\text{left/right},i}$ is the probability of a positron on layer boundary i to jump to the left or right adjacent layer boundary (with 0 being the surface and $j_{\text{right},0} = 0$). Note that the surface here is both a boundary (in the sense that

positrons can diffuse there) and a layer (in the sense that positrons can annihilate there), and is assumed to be infinitely attractive. The matrix, \mathbf{R} , is filled with the probabilities of transitions from transient to absorbing states, i.e., positrons annihilating in a layer (including the surface). For the above example:

$$\mathbf{R} = \begin{pmatrix} 1 & 0 & 0 & 0 \\ 0 & a_{\text{left},1} & 0 & 0 \\ 0 & a_{\text{right},1} & a_{\text{left},2} & 0 \\ 0 & 0 & a_{\text{right},2} & a_{\text{left},3} \\ 0 & 0 & 0 & a_{\text{right},3} \end{pmatrix}, \quad (19)$$

where $a_{\text{left/right},i}$ is the probability of a positron on layer boundary i to annihilate in the left or right layer of the boundary. The matrix of absorption probabilities can be calculated as

$$\mathbf{B} = \mathbf{R} \cdot \sum_{n=0}^{\infty} \mathbf{Q}^n = \mathbf{R} \cdot (\mathbf{I} - \mathbf{Q})^{-1}, \quad (20)$$

where we utilize the geometric series, and the resulting annihilation fractions per layer (and surface) for a given energy E are

$$\vec{n}_{\text{ann}} = \mathbf{B} \cdot \vec{n} + \vec{f}_{\text{ann}}, \quad (21)$$

with the remaining positrons on boundaries, \vec{n} , and the already annihilated positrons, \vec{f}_{ann} , from the first diffusion step. The lineshape parameter S results from a weighted sum of all layer- and surface-specific lineshape parameters

$$S = \vec{n}_{\text{ann}} \cdot \vec{S} = \sum_{i=1}^N S_i n_i + S_{\text{surf}} n_{\text{surf}}, \quad (22)$$

where N is the number of layers.

2.4 Depth Profiles

Modelling diffusion and calculating annihilation profiles for multiple positron implantation energies yields a so-called depth profile:

$$S(E) = \sum_{i=1}^N S_i n_i(E) + S_{\text{surf}} n_{\text{surf}}(E). \quad (23)$$

Fitting this model function to data obtained from depth-resolved DBS experiments allows the extraction of the positron diffusion length and other parameters.

2.5 Positron Affinity

The positron affinity, A_+ , quantifies how strongly positrons are attracted or repelled by different materials. Values of the element dependent A_+ can be calculated from the chemical potential of electrons and positrons in the material and can be found in literature for a selection of materials [PLN89]. The positron affinity affects the mobility of positrons in layered systems and alloys with precipitates. To account for the positron affinity, all diffusion and annihilation probabilities in the second step of modelling the diffusion ($a_{\text{left/right}}$, $j_{\text{left/right}}$, see section 2.3) are multiplied by a Boltzmann factor,

$$\exp \left[- \frac{A_+}{k_B T} \right], \quad (24)$$

where k_B is the Boltzmann constant and T the temperature, and subsequently normalized.

2.6 Epithermal Correction

A fraction of positrons may annihilate before complete thermalization with epithermal energy. LIMPID contains an optional simple correction to account for epithermal positrons as suggested by [BRE88] and previously used by [Vee+91]. It introduces an additional lineshape parameter value, S_{epi} , and an average epithermal scattering length, L_{epi} . The scattering length L_{epi} is typically in the order of 1 nm and, like any other variable, can either be fixed or varied during the fitting procedure. The resulting $S(E)$ profile, including the epithermal correction, is given by

$$S(E) = S_{\text{epi}} \eta_{\text{epi}}(E) + (1 - \eta_{\text{epi}}(E)) \left[\sum_{i=1}^N S_i n_i(E) + S_{\text{surf}} n_{\text{surf}}(E) \right], \quad (25)$$

with the fraction of epithermal positrons,

$$\eta_{\text{epi}} = \int_0^\infty P(z, E) \exp \left[- \frac{z}{L_{\text{epi}}} \right] dz. \quad (26)$$

3 Results / Example Application

In this example, we use LIMPID to analyze DBS data obtained from measuring a Cu layer deposited on a Si substrate [Koh22]. The Cu layer has been electron-beam physical vapor-deposited on B-doped Si with dimensions $10 \times 10 \times 0.4 \text{ mm}^3$ with a deposition rate of $\approx 0.1 \text{ nm/s}$. We calculate the positron implantation and annihilation fractions inside the layer structure. Implantation profiles are calculated using the Makhov function (Equation 1) with the material-specific parameters listed in Table 1. The S parameter value for the Si substrate, as well as the positron diffusion length in Si, are known from LIMPID fits to measurement data of a bare Si substrate. They are listed in Table 2 and fixed for the fit. The epithermal scattering length is fixed to $L_{\text{epi}} = 1 \text{ nm}$.

Table 1: Material-specific Makhov parameters and positron affinities for Cu and Si taken from literature [DH08; PLN89].

	$\rho / \text{g cm}^{-3}$	$A / \mu\text{g cm}^{-2} \text{ keV}^{-n}$	m	n	A_+ / eV
Cu	8.96	2.84	1.73	1.67	-4.81
Si	2.33	2.48	1.99	1.73	-6.95

Table 2: A list of fixed and varied LIMPID fit parameters used for the Cu/Si system. The best-fit values on the left include the correct positron affinities and an epithermal correction. Note that the “values w/o affinities” correspond to a direct fit with no positron affinities provided and therefore do not relate to the red curve in Figure 4 or the last fraction plot in Figure 6.

	Value	Type	Value w/o epithermal corr.	Value w/o affinities
S_{epi}	0.6308 ± 0.0005	varied	—	0.6309 ± 0.0006
S_{surf}	0.6208 ± 0.0006	varied	0.6269 ± 0.0005	0.6205 ± 0.0006
S_{Cu}	0.5786 ± 0.0004	varied	0.5801 ± 0.0006	0.5775 ± 0.0005
S_{Si}	0.6659	fixed	0.6659	0.6659
L_{epi}	1 nm	fixed	—	1 nm
L_{Cu}	$(30.4 \pm 1.2) \text{ nm}$	varied	$(23.2 \pm 0.9) \text{ nm}$	$(32.1 \pm 1.3) \text{ nm}$
L_{Si}	386 nm	fixed	386 nm	386 nm
d_{Cu}	$(448 \pm 3) \text{ nm}$	varied	$(448 \pm 5) \text{ nm}$	$(330 \pm 3) \text{ nm}$

The free fit parameters and their best values are listed in Table 2 as type “varied”. The Cu diffusion length, $L_{\text{Cu}} = 30.4 \text{ nm}$, appears to be short but reasonable for a vapor-deposited, presumably unordered and defect-rich layer. The 448 nm layer thickness is close to what we aimed for with the vapor deposition duration ($\approx 500 \text{ nm}$). Comparing the fit with and without positron affinities (see Table 2) shows the value of the LIMPID feature. Both variations result in a nearly identical fit (see the “best fit” line in Figure 4), but the fit without positron affinities, i.e., assuming equal values for all materials, results in a slightly larger value for the positron diffusion length in Cu, $L_{\text{Cu}} = 23.2 \text{ nm}$, and a significantly smaller layer thickness, $d_{\text{Cu}} = 330 \text{ nm}$. The fit with epithermal correction disabled yields similar results for diffusion length and layer thickness, but ceases to match the data towards low implantation energies $\leq 3 \text{ keV}$, as can be seen in Figure 4: It shows the measured S parameter as a function of the positron implantation energy for the Cu/Si system, along with the corresponding LIMPID fit. Note that we did not include the fit without affinities, for it is identical to the best fit. Instead, we include an affinity-less model of the best-fit results (see the red line in Figure 4) to illustrate the impact of the feature. Modeling positron diffusion using the best fit results, but with the positron affinities set equal, $A_+^{\text{Si}} = A_+^{\text{Cu}}$, results in this significant deviation towards higher energies. This can be attributed to the fraction of positrons diffusing from the (more attractive) Si towards Cu being reduced due to their different affinities compared to the affinity-less case.

As a result of the fit, we can use LIMPID to visualize the multi-layer implantation profiles and the fractions of positrons annihilating in each channel. Figure 5 shows two exemplary implantation profiles for the positron implantation energies 12 and 27 keV. The distinct profiles for both materials are calculated separately and concatenated in a way that assures the correct fractions in each layer and that they sum to 1. As a result, we get jump discontinuities at the layer boundaries.

Figure 6 contains fraction plots of the implanted positrons and the different annihilation channels. It aids in understanding the impact of different parameters, such as densities, layer thicknesses, and positron affinities, on other fit results. The impact of using positron affinities, for example, can be seen by comparing the crossing point of the Cu

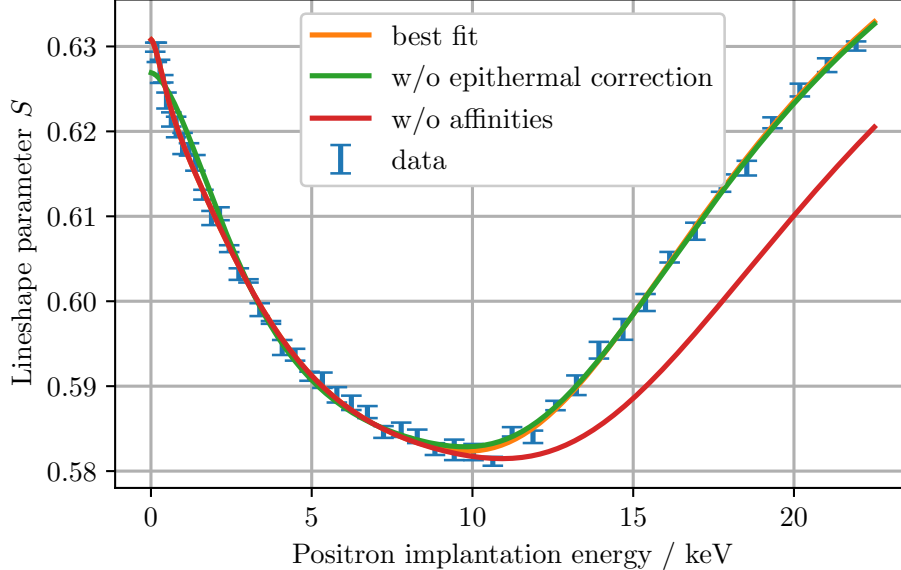


Figure 4: Depth-resolved DBS data for a Cu layer on a Si substrate, fitted using the LIMPID algorithm. The experimental data (symbols) and LIMPID models (solid lines) demonstrate almost perfect agreement for the $S(E)$ profile. The orange line represents the best fit achieved (and is identical for the fit without positron affinities) using the correct positron affinities and an epithermal correction. The green line shows a fit with the epithermal correction disabled, resulting in significant deviation for energies ≤ 3 keV. The red line shows an affinity-less model of the best-fit result. All fit parameters are listed in Table 2.

(green) and Si (red) fraction curves in all three fraction plots. From top to center, the higher positron affinity of Si shifts the crossing point towards lower implantation energies, i.e., increases the fraction of positrons annihilating in Si. Equal affinity values for Cu and Si (bottom) shift the crossing point towards higher energies (even further than for the implantation profile).

4 Conclusion

We have presented LIMPID, a versatile computational tool for modeling positron diffusion and annihilation profiles in layered materials. By integrating well-established implantation models and a Markov chain approach to diffusion, LIMPID provides accurate fits to depth-resolved DBS data. Future developments will, amongst others, focus on extending support for anisotropic materials (mainly defect distributions), offering the possibility for a second surface (i.e., finite thickness samples), and adding more models for positron implantation.

Acknowledgment

Financial support by the German Research Foundation (DFG) within the Project HU 978/19-1 is gratefully acknowledged.

References

- [Aer94] G. Aers. “Positron stopping profiles in multilayered systems”. In: *Journal of applied physics* 76.3 (1994), pp. 1622–1632.
- [AL90] P. Asoka-Kumar and K. Lynn. “Implantation profile of low-energy positrons in solids”. In: *Applied physics letters* 57.16 (1990), pp. 1634–1636.
- [BRE88] D. Britton, P. Rice-Evans, and J. Evans. “Epithermal effects in positron depth profiling measurements”. In: *Philosophical magazine letters* 57.3 (1988), pp. 165–169.

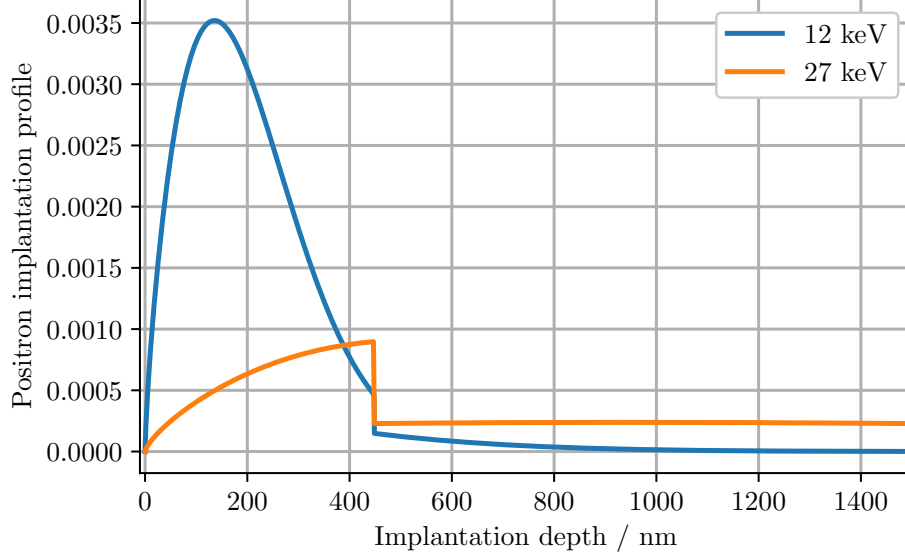


Figure 5: Calculated positron implantation profiles in the Cu/Si sample for two representative positron implantation energies (12 keV and 27 keV). We used the thicknesses resulting from the best fit in Figure 4 and Table 2, i.e., 448 nm Cu on top of the Si substrate. The profiles show how the implantation depth and spread depend on energy and (mainly) how density shapes multi-layer implantation.

- [Bur+25] V. V. Burwitz, A. Kärcher, L. Mathes, A. Book, N. Paul, T. Schwarz-Selinger, M. Butterling, E. Hirschmann, M. O. Liedke, A. Wagner, E. Unsal, G. Cuniberti, and C. Hugenschmidt. “Tungsten oxide thin films probed by depth-resolved positron annihilation spectroscopy”. In: *Phys. Rev. B* 111 (5 2025), p. 054114. DOI: 10.1103/PhysRevB.111.054114.
- [Číž18] J. Čížek. “Characterization of lattice defects in metallic materials by positron annihilation spectroscopy: A review”. In: *Journal of Materials Science & Technology* 34.4 (2018), pp. 577–598.
- [DH08] J. Dryzek and P. Horodek. “GEANT4 simulation of slow positron beam implantation profiles”. In: *Nuclear Instruments and Methods in Physics Research Section B: Beam Interactions with Materials and Atoms* 266.18 (2008), pp. 4000–4009.
- [Gho95] V. Ghosh. “Positron implantation profiles in elemental and multilayer systems”. In: *Applied surface science* 85 (1995), pp. 187–195.
- [Har+20] C. R. Harris, K. J. Millman, S. J. van der Walt, R. Gommers, P. Virtanen, D. Cournapeau, E. Wieser, J. Taylor, S. Berg, N. J. Smith, R. Kern, M. Picus, S. Hoyer, M. H. van Kerkwijk, M. Brett, A. Haldane, J. F. del Río, M. Wiebe, P. Peterson, P. Gérard-Marchant, K. Sheppard, T. Reddy, W. Weckesser, H. Abbasi, C. Gohlke, and T. E. Oliphant. “Array programming with NumPy”. In: *Nature* 585.7825 (2020), pp. 357–362. DOI: 10.1038/s41586-020-2649-2.
- [Hun07] J. D. Hunter. “Matplotlib: A 2D graphics environment”. In: *Computing in Science & Engineering* 9.3 (2007), pp. 90–95. DOI: 10.1109/MCSE.2007.55.
- [Koh22] B. Kohlhaas. “Characterization of metallic thin-film systems by depth-dependent Doppler-broadening spectroscopy of the positron annihilation line”. Bachelor’s Thesis. Technical University of Munich, 2022.
- [Mak60] A. Makhov. “The penetration of electrons into solids, II. The distribution of electrons in depth”. In: *Fizika Tverdogo* 2.9 (1960), pp. 2172–2175.
- [New+24] M. Newville, R. Otten, A. Nelson, T. Stensitzki, A. Ingargiola, D. Allan, A. Fox, F. Carter, Michał, R. Osborn, D. Pustakhod, S. Weigand, Ineuhaus, A. Aristov, Glenn, Mark, mgunyho, C. Deil, A. L. R. Hansen, G. Pasquevich, L. Foks, N. Zobrist, O. Frost, Stuermer, J.-C. Jaskula, S. Caldwell, P. Eendebak, M. Pompili, J. H. Nielsen, and A. Persaud. *lmfit/lmfit-py*: 1.3.2. Version 1.3.2. 2024. DOI: 10.5281/zenodo.12785036.
- [PLN89] M. Puska, P. Lanki, and R. Nieminen. “Positron affinities for elemental metals”. In: *Journal of Physics: Condensed Matter* 1.35 (1989), p. 6081.
- [PN94] M. J. Puska and R. M. Nieminen. “Theory of positrons in solids and on solid surfaces”. In: *Reviews of modern Physics* 66.3 (1994), p. 841.

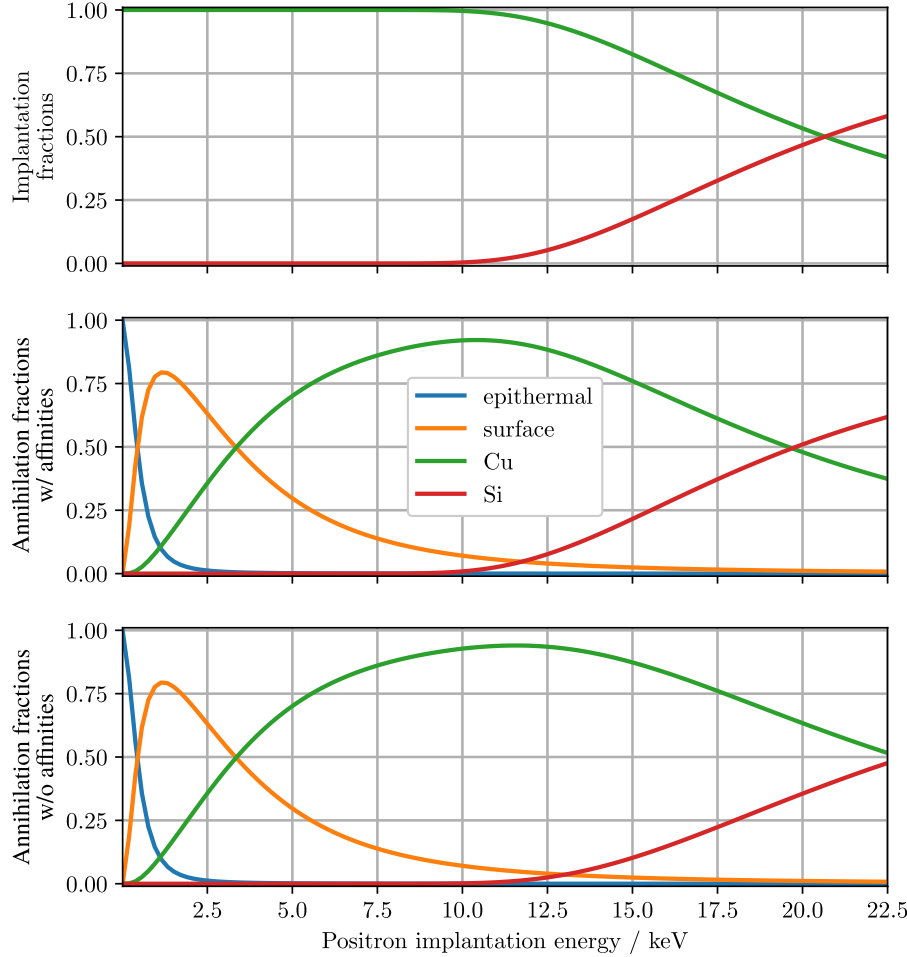


Figure 6: Fractions of positrons implanted and annihilated in different channels as a function of implantation energy. Top: Implantation fractions in each layer. Center: Corresponding annihilation fractions for the best fit results resolved into epithermal annihilation, surface annihilation, and annihilation in Cu and Si. Bottom: Corresponding annihilation fractions for an affinity-less model of the best-fit results.

- [Sch+24] N. Schalk, Y. Moritz, G. K. Nayak, D. Holec, C. Hugenschmidt, V. V. Burwitz, L. Mathes, M. Schiester, C. Saringer, C. Czettl, M. Pohler, C. Mitterer, and M. Tkadletz. “Nanocomposite versus solid solution formation in the TiSiN system”. In: *Acta Materialia* 275 (2024), p. 120063. ISSN: 1359-6454. DOI: <https://doi.org/10.1016/j.actamat.2024.120063>.
- [SL88] P. J. Schultz and K. G. Lynn. “Interaction of positron beams with surfaces, thin films, and interfaces”. In: *Reviews of Modern Physics* 60.3 (1988), p. 701.
- [Vee+91] A. v. Veen, H. Schut, J. d. Vries, R. A. Hakvoort, and M. R. Ijppma. “Analysis of positron profiling data by means of “VEPFIT””. In: *AIP Conference Proceedings* 218.1 (1991), pp. 171–198. ISSN: 0094-243X. DOI: [10.1063/1.40182](https://doi.org/10.1063/1.40182). eprint: https://pubs.aip.org/aip/acp/article-pdf/218/1/171/12126267/171_1_online.pdf.
- [Veh+87] A. Vehanen, K. Saarinen, P. Hautojärvi, and H. Huomo. “Profiling multilayer structures with monoenergetic positrons”. In: *Physical Review B* 35.10 (1987), p. 4606.
- [Vir+20] P. Virtanen, R. Gommers, T. E. Oliphant, M. Haberland, T. Reddy, D. Cournapeau, E. Burovski, P. Peterson, W. Weckesser, J. Bright, S. J. van der Walt, M. Brett, J. Wilson, K. J. Millman, N. Mayorov, A. R. J. Nelson, E. Jones, R. Kern, E. Larson, C. J. Carey, İ. Polat, Y. Feng, E. W. Moore, J. VanderPlas, D. Laxalde, J. Perktold, R. Cimrman, I. Henriksen, E. A. Quintero, C. R. Harris, A. M. Archibald, A. H. Ribeiro, F. Pedregosa, P. van Mulbregt, and SciPy 1.0 Contributors. “SciPy 1.0: Fundamental Algorithms for Sci-

entific Computing in Python”. In: *Nature Methods* 17 (2020), pp. 261–272. DOI: 10.1038/s41592-019-0686-2.